Experimental study to identify premonitory factors of landslide dam failures

Fawu Wang[a,][*], Zili Dai[a], Chukwueloka Austin Udechukwu Okeke[b], Yasuhiro Mitani[a], Hufeng Yang[c]

[a] Department of Earth Science, Faculty of Natural Science, Shimane University, 1060 Nishikawatsu-cho, Matsue, Shimane 690-8504, Japan
[b] Department of Civil Engineering, College of Engineering, Covenant University Ota, Ogun State, Nigeria
[c] Department of Geological Engineering, Faculty of Geosciences and Environmental Engineering, Southwest Jiaotong University, Chengdu, China

ARTICLE INFO

ABSTRACT

Identifying premonitory factors before final failure for long-existing landslide dams is of high importance in disaster prevention and risk reduction. In this study, a series of large-scale (outdoor) experiments were designed and conducted to identify premonitory factors that may be used in failure prediction for actual landslide dams. Surface deformation, especially dam-crest settlement, dam seepage-water turbidity and self-potential across the dam crest were selected as the target parameters. Changes in these parameters showed apparent correlations between each other. Based on the monitoring data obtained and the observation performed during the tests, the deformation and failure sequence of the dam model can be separated into four time-sequential periods: 1) Emergence of seepage water and front wetting. In this period, the monitoring parameters did not show any obvious changes. However, wetting was observed in the downstream face. 2) Hyperconcentrated flow discharge. In this period, water flowed out of the drainage channel, and the vertical deformation of the dam body became obvious, while the turbidity of the seepage water increased. 3) Emergence and development of cracks on the dam crest. In this period, the dam-crest settlement also increased. 4) Sudden collapse and final failure. In this period, self-potential across the dam crest decreased rapidly, and the dam-crest settlement reached a peak value. Therefore, dam-crest settlement, seepage-water turbidity and self-potential changes can be regarded as premonitory factors of landslide dam failure.

1. Introduction

Landslides and rock avalanches can result in natural damming of stream channels and gorges. Such events are common in many mountainous regions where several geomorphological and hydroclimatic factors favour the occurrence of geomorphic processes such as landslide dams (Hewitt, 1982; Hermanns et al., 2004). Once a landslide dam is formed, breaching can occur, resulting in the release of lake water impounded upstream of the dam. Failure of landslide dams often trigger outburst floods with potentially catastrophic effects in downstream areas (Evans, 1986; Costa and Schuster, 1991; Casagli and Ermini, 1999; Bovis and Jakob, 2000; Dai et al., 2005; Hancox et al., 2005; Korup and Tweed, 2007; O'Connor and Beebee, 2009). Therefore, a better understanding of premonitory factors, especially those that can be easily measured or observed in actual landslide dams at high risk of failure, is important for disaster reduction.

The probability of landslide dam failure remains an integral part of flood-risk modelling and hazard-assessment studies. Costa and Schuster (1988) reported that the longevity of landslide dams depends on several

factors including the rate of seepage through the dam; the internal structure and material properties of the dam; the size, shape and volume of the blockage; and the rates of sediment and water flow into the upstream lake. Piping and internal erosion due to seepage flow are among the major failure modes of landslide dams. For example, the failure in 2004 of the Tsatichhu landslide dam in Bhutan was due to dam-face saturation and progressive seepage (Dunning et al., 2006), while seepage-induced instabilities were identified in the debris-avalanche dam at Castle Lake near Mount St Helens, Washington (Meyer et al., 1994), in the Bairaman landslide dam in Papua New Guinea (King et al., 1989) and in glacial moraine dams in Peru (Vilimek et al., 2005). Therefore, seepage flow can be regarded as one of the common triggering factors of landslide dam failure.

Numerous attempts have been made to investigate the complex mechanisms of piping and internal erosion in landslide dams, including theoretical analyses and experimental studies (Ojha et al., 2008; Amaya et al., 2009; Vorogushyn et al., 2009). In their theoretical research, for instance, Bonelli and Benahmed (2010) proposed a simplified mechanically-based approach for the prediction of piping failure in

cohesive dams. However, this approach is only applicable in dams formed of cohesive materials of high plasticity that are capable of supporting the roof of the piping hole. ICOLD (2013) proposed four most important premonitory indices for the assessment of the hydraulic behaviour of dams: (1) the magnitude and variation of pore-water pressures, (2) the rate, magnitude and location of internal and external deformations, (3) the amount, location, turbidity and origin of seepage in the dam, and (4) the magnitude and rate of settlement. Similarly, Fell et al. (2005) described some primary features observed in embankment dams in the early stages of piping, including the presence of muddy leakages, sand boils, settlements, cracking, whirlpools in the reservoir, sinkholes and the development of high pore-water pressures.

Physical model tests are widely used to investigate the failure mechanism of landslide dams. To enhance the understanding of landslide-dam-break flooding, Yan et al. (2009) carried out a series of flume experiments over an erodible bed, in which overtopping flow of the dam caused the dam to fail during the tests. Cao et al. (2011) conducted a total of 28 runs of flume experiments with differing inflow discharges, dam compositions, dam geometries and initial breach dimensions, and stated that dam failure was primarily caused by erosion due to overtopping flow, and lateral mass collapse was also considerable during the process of breach widening. Balmforth et al. (2008) presented an experimental study to observe the catastrophic erosional incision of a moraine dam caused by a large displacement wave. Previous experimental studies have thus mostly focused on dam failure triggered by overtopping flow, and the effects of seepage have not been much analysed. Furthermore, previous physical experiments have been constrained by their comparatively small spatial scales (e.g., Zhu et al., 2006; Balmforth et al., 2008; Balmforth et al., 2009) and therefore may not be able to fully reveal the complicated failure mechanism of landslide dams.

The main objective of this research is to identify the premonitory factors of landslide dam failure induced by seepage through the landslide dam. To achieve this objective, large-scale (outdoor) physical experiments were performed using different kinds of precision sensors and geophysical methods to obtain real data representing the deformation behaviour of the landslide dam models.

To facilitate the possible applications of this study to actual landslide dam problems, multiple approaches were designed to measure the premonitory factors. Fig. 1 shows a conceptual model of the experimental study on landslide dam failure. A GPS sensor to monitor dam-crest settlement was scheduled for practical use. However, for high precision during the test, it was replaced by laser sensors. The following factors were considered as the targets:

1) Dam-crest settlement, which can represent the surface deformation and can be easily monitored by GPS or InSAR;
2) Vertical deformation inside the dam body;
3) Turbidity of seepage water at the downstream side;
4) Self-potential change, which results from seepage flowing and can be easily monitored across the dam crest;

5) Hydraulic gradient, which is the main parameter controlling hydrodynamic conditions, and can be monitored by a set of water-pressure transducers.

2. Experimental methods

2.1. Experimental setup and site description

The experiments were performed in a research facility located on Eshima Island (35°30′30″ N, 133°11′38″ E), about 20 km northeast of Matsue city, Shimane Prefecture, Japan (Fig. 2). The experimental facility comprised a rectangular barrier of 13.4 m length, 10.2 m width, and 1.7 m height, with an open end for the construction of the landslide dam models (see Fig. 3). The rectangular barrier was constructed of soil material, and several layers of tarpaulin sheets were used to cover the internal (reservoir area) and external parts of the barrier to minimize seepage and rainfall infiltration. The barrier was constructed such that the internal and external slope ratios were fixed at 1.5H:1 V and 1H:1 V, respectively. The upstream lake was recharged via a drainage hose connected to a local water main. Transient variation in the upstream reservoir was monitored using a 50 kPa capacity pore-pressure transducer. Fig. 4 shows the layout of the dam model. Internal erosion and piping were initiated by laying uniform gravel and cobbles in a near-square channel of 0.2 m width, 0.3 m above the dam bottom. The geometrical characteristics of the dam models are shown in Fig. 4. H and L represent the dam height and the dam-crest length, respectively, while α and β represent the upstream and downstream slope angles, respectively. As shown in Fig. 5, the drainage channel comprised gravel and cobbles. Four pore-pressure transducers (hereinafter referred to as PWP-1, PWP-2, PWP-3, and PWP-4) were inserted above the artificial drainage channel to monitor the water pressure along the longitudinal section of the dam model, and the values were used to calculate the hydraulic gradient, which can represent the hydrodynamic condition of the landslide dam model. To evaluate vertical deformation inside the dam body, a flexible PVC pipe (0.075 m in diameter) was buried in the dam parallel to the strike direction of the dam, about 0.5 m above the artificial drainage channel. Four strain gauges (hereinafter referred to as VD-1, VD-2, VD-3 and VD-4) were attached to the upper surface of the PVC pipe, as shown in Fig. 4(b). Therefore, the vertical deformation (VD) behaviour of the central part of the dam body could be evaluated through the deformation of the PVC pipe, although no deformation could be measured if the PVC pipe settled homogeneously with the dam body. Dam-crest settlement (relative to the two barriers of the dam model) was monitored by two multifunctional analogue laser displacement sensors, which were suspended by a cylindrical metallic rod fixed over the dam crest. As shown in Fig. 4 and Fig. 6, one displacement sensor was positioned on the central axis of the dam, and the other was positioned on its right-hand side at a horizontal distance of 1.0 m ("right-hand side" in this paper is the right-hand side when facing downstream on the dam model). The laser displacement sensors are hereinafter referred to as S_d-Central and S_d-Right. Self-potential
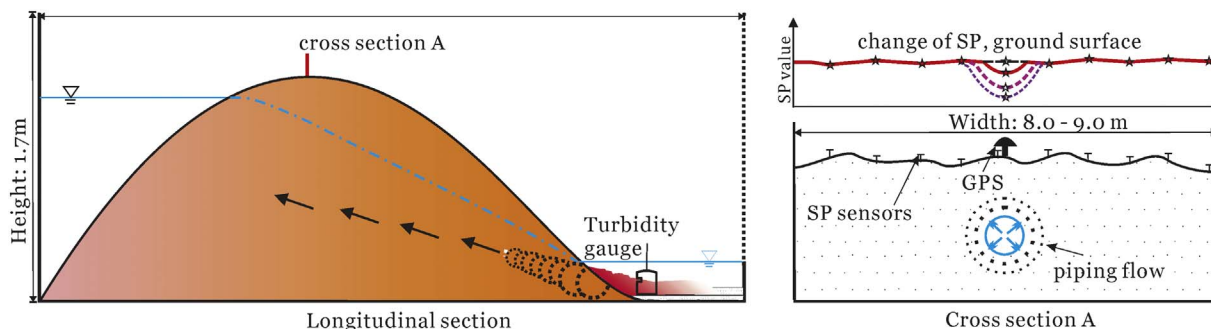

Fig. 1. Conceptual model of the experimental study on landslide dam failure.

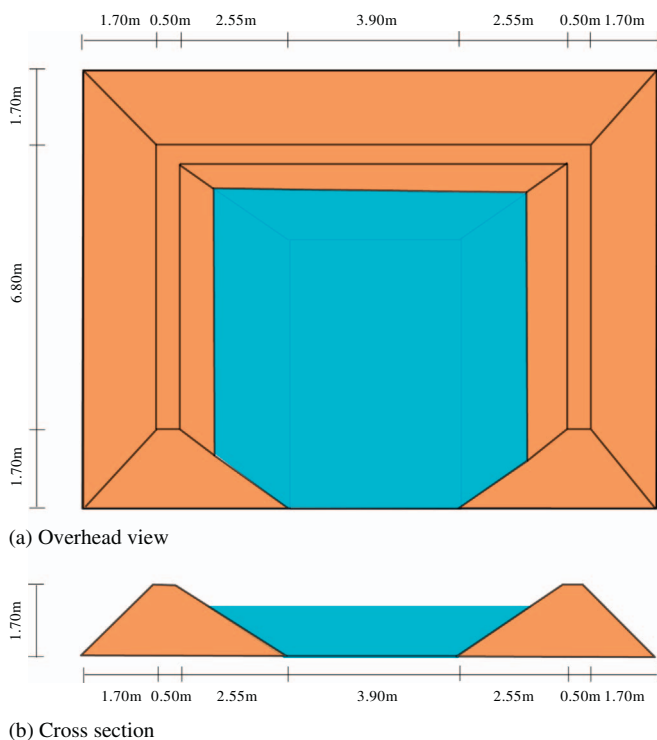(a) Overhead view

(b) Cross section

**Fig. 3.** Layout of the artificial reservoir surrounded by barrier: (a) overhead view; (b) cross section.

measurements using six electrodes positioned across the dam crest were performed to monitor the self-potential changes caused by the water flowing through the dam body. The electrode locations are shown in Fig. 4(b). The turbidity of seepage water was measured using a turbidity sensor (model: VisoTurb[R] 700 IQ SW) installed near the possible exit point of the seepage water (Fig. 7). It was expected that internal erosion process would start with the selective removal of fines within the interstitial pores of sand materials. The turbidity sensor measured the amount of light scattered by the suspended solids in the water. The turbidity level (cloudiness or haziness) of the seepage water increases as the amount of total suspended solids in the water increases. All the sensors were connected to a standard real-time monitoring and recording unit comprising a universal recorder (KYOWA EDX-100A) and a laptop computer.

## 2.2. Soil characteristics and dam model construction

The material used to build the dam model was sourced from the Mihata landslide, which occurred on 6 August 2012 in the Mihata district, near Izumo city, Shimane Prefecture, Japan. This landslide had dammed a small valley and formed a small-scale landslide dam. The material consists of highly weathered igneous and sedimentary rocks including andesite, rhyolite, sandstone and mudstone. The soil consists of 35.5% gravel, 37.5% sand, 20.9% silt and 6.1% clay particles. The grain-size distribution curves of the materials are shown in Fig. 8. The average coefficient of curvature, coefficient of uniformity and effective grain size of the soil were 3.33, 1333, and 0.003 mm, respectively. After the dam models were constructed, soil samples were taken from the dam face, and the physical properties of the soil material were obtained through a series of laboratory tests. The sampling-point locations are shown in Fig. 6, and the test data are shown in Table 1. The bulk density and dry density ranged from 1355 to 1660 kg/m^3 and 979–1359 kg/m^3, respectively. The specific gravity of the soil material was around 2.7. The void ratio of the soil ranged from 0.978 to 1.695. To simulate the loose structure of the landslide dam caused by the Mihata landslide, no compaction was applied during the dam model construction. The water content was about 21.0%, and the degree of saturation ranged from 31.8% to 60.7%. The plastic limit (*PL*), liquid limit (*LL*), and the plasticity index (*PI*) were 39%, 58% and 19%, respectively. Therefore, the erosion resistance of the soil sample was classified as Category 1 (greatest piping resistance) according to the classification standard proposed by Sherard (1953).

The strength parameters of the soil materials are important for the stability analysis of the slopes, and can be obtained through various laboratory tests, especially the triaxial test (Lade, 1992; Nova, 1994; Daouadji et al., 2011; Nicot et al., 2007). Since the presented work focuses on the post-failure behaviour of the landslide dam model, a simple in-situ test known as the portable dynamic cone penetration test (PDCPT) was carried out on the dam crest to estimate the strength behaviour of the soils. The PDCPT uses a metal hammer of 5 kg freely falling from 500 mm height to drive a rod into the ground. A cone with an angle of 60° and a width of 25 mm is fixed at the end of the 16-mm-diameter rod. The length of each rod is 500 mm, and the total length penetrating the ground can reach 4 m. The cone and rod are made of stainless steel. The number of hammer blows required to drive the cone 100 mm into the ground is recorded as the N_c-value. The N_c-value can be empirically equal to 0.5 *N*, in which *N* is the value obtained from the standard penetration test (SPT).

The locations of the tests are shown in Fig. 6 by the labels PDCPT-a,
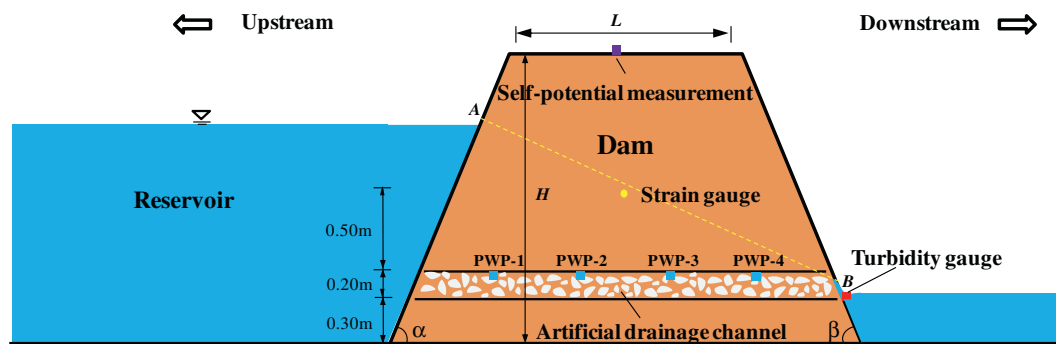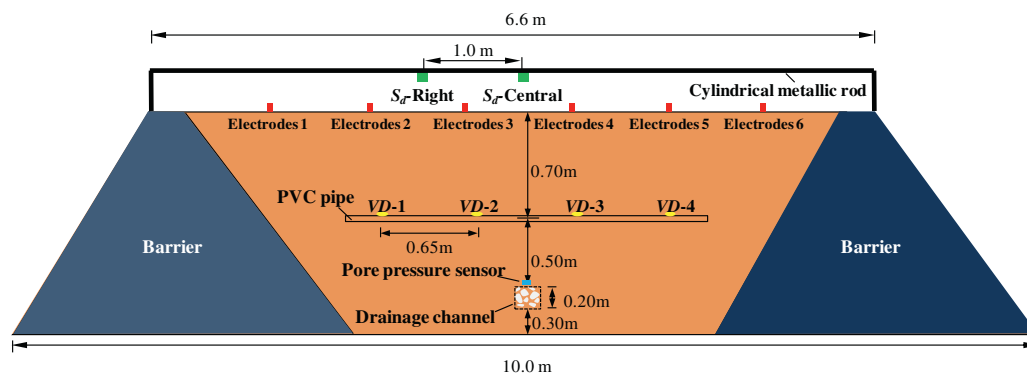
Fig. 4. Layout of the landslide dam model: (a) longitudinal section; (b) cross section.

Fig. 5. Artificial drainage channel in the landslide dam model.

PDCPT-b and PDCPT-c. The blow-counts-versus-depth test results are shown in Fig. 9. The results show that for the soil material within 1.8 m of the dam crest, most of the N_c-values are less than 5, and the average N_c-value is about 3, indicating that the soil material is very loose. Combining the above physical parameters indicates that the soil material used in these tests was poorly compacted and with low shear strength.

In the large-scale (outdoor) experiments, the landslide dam models were constructed using a mini-excavator and other heavy-duty equipment. In the early stages, a hand-propelled vibratory plate compactor was used to compact the ground to ensure homogeneity of the underlying foundation material. Subsequently, to simulate the formation process of landslide dams, the soil material from the Mihata landslide was placed by the mini-excavator in equal layer.

The experiment started with the filling of the upstream reservoir. The discharge into the reservoir was maintained until the reservoir level reached a maximum level considered safe for the operation of the dam. Subsequently, an equilibrium hydraulic head was maintained by establishing a constant water level. In all the experimental runs, a large channel was excavated at the toe of the downstream slope to minimize backwater flooding and to ensure accurate readings from the turbidity sensor.

3. Results and discussion

In this work, four outdoor tests were carried out to investigate the premonitory factors of landslide dam failure. The geometrical shapes of the four landslide dam models are listed in Table 2. Experiment 1 investigated the effect of pore-water pressure and hydraulic gradient on internal erosion in the landslide dam model. Experiments 2 and 3 examined the relationships between dam-body deformation, dam-crest settlement and seepage-water turbidity. Experiment 4 measured self-potential during the seepage process, and the relationship between dam-crest settlement and seepage-water turbidity was analysed.

With the filling of the upstream reservoir, the dam material was partially saturated, and the difference in water head between the upstream and downstream sides of the dam resulted in seepage in the landslide dam model. The failure sequence of the landslide dam model is shown in Fig. 10. The rapid rise in pore-water pressures from the upstream side to the down stream side of the dam model resulted in the water gushing out of the artificial drainage channel, and the upslope propagation of the wetting front on the downstream face of the

Fig. 7. Turbidity sensor to monitor the rate of internal erosion and piping.

Fig. 8. Grain-size distribution curves of the landslide materials used in the experiments.

Table 1
Physical properties of the materials used in the experiments.

Sample number	Bulk density (kg/m³)	Dry density (kg/m³)	Specific gravity (/)	Water content (%)	Void ratio (/)	Degree of saturation (%)
1	1646	1358	2.688	21.1	0.978	58.0
2	1398	1150	2.725	21.6	1.370	43.0
3	1179	979	2.639	20.4	1.695	31.8
4	1355	1124	2.682	20.5	1.385	39.7
5	1660	1359	2.773	22.8	1.041	60.7
6	1510	1288	2.674	21.2	1.075	42.8

although wetting was observed on the downstream face. Seepage water emerged at the downstream face, and the wetting front propagated upwards. 2) Hyperconcentrated flow discharge. This moment is defined as T_B. In this period, water flowed out of the drainage channel, and the vertical deformation of the dam body became obvious, while the turbidity of the seepage water increased. 3) Emergence and development of cracks on the dam crest. This moment is defined as T_C. In this period, cracks emerged and developed on the dam crest, and the dam-crest settlement increased. 4) Sudden collapse and final failure of the dam model at moment T_D, together with a sharp increase in dam-crest settlement.

3.1. Experiment 1

Landslide dams are predominantly unsaturated or partially saturated, hence the presence of matric suction (negative pore-water pressure) induces an apparent cohesion that increases the stability of landslide dams. However, the discharge of the upstream reservoir resulted in the reduction of the matric suction, which in turn resulted in an internal instability. In addition, the formation of a lake on the upstream side of a landslide dam can lead to the development of high water pressure, which may initiate internal erosion and progress to form a piping hole. Fig. 11 shows the evolution of the upstream water level and pore-water pressures monitored by the four sensors in the landslide dam model (see Fig. 4) in Experiment 1. The pore-water pressures in the landslide dam model increased with the water level in the upstream reservoir. The maximum values of PWP-1, PWP-2, PWP-3, and PWP-4 were as high as 11.8 kPa, 9.8 kPa, 5.9 kPa and 1.7 kPa, respectively. The increasing pore-water pressures can cause a reduction in the resisting forces of the dam materials. The water pressure differences can result in seepage force, which can result in the mobilization and downstream entrainment of soil particles towards an unprotected exit at the downstream face.
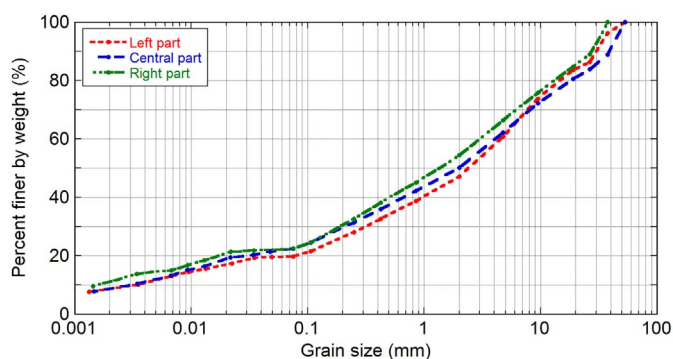
landslide dam model. The high seepage gradient developed from the upstream side to the down stream side of the dam, and then caused abrupt erosion and outwash of the dam materials to an exit point on the downstream face, leading to the cracking and settling of the dam crest. Therefore, the failure sequence of the dam model could be generally divided into four periods. These four periods, and the critical moments marking their beginnings, are defined as follows: 1) Emergence of seepage water and front wetting. This moment is defined as T_A. In this period, the monitoring parameters did not show any obvious changes,
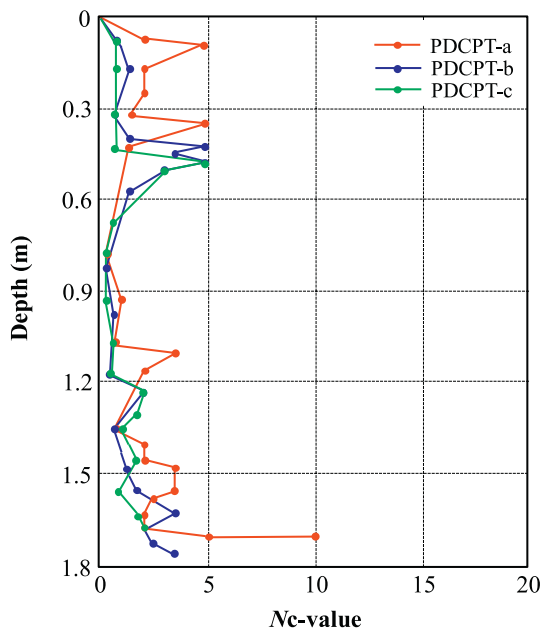
Fig. 9. Results of portable dynamic cone penetration tests (PDCPTs) on the dam crest in Experiment 4.

Table 2
Geometrical shapes of the landslide dam models in the experiments.

Experiment	Dam height (m)	Dam crest length (m)	Upstream slope angle (°)	Downstream slope angle (°)
1	1.70	0.85	39	37
2	1.91	0.91	39	38
3	1.98	0.89	41	38
4	1.80	0.80	40	40

Seepage-water turbidity has been identified as one piece of direct evidence of internal erosion in engineered dams and landslide dams. Muddy water that contains a significant amount of suspended soil particles (sediments) is indicative of the evolution of internal erosion and piping. According to Brown and Gosden (2008), the significant premonitory factor for early warning of internal erosion and piping in dams is turbidity of seepage flows. In this study, we collected the muddy water and tried to make grain-size distribution analysis of the soil material brought out by the seepage flow. This trial was abandoned because of the low turbidity of the muddy water. The collected soil mass was not sufficient for the analysis even though several buckets were used to store the muddy water. Fig. 12 shows the trends of the hydraulic gradient and variation in turbidity of the seepage water in Experiment 1. Strictly speaking, the hydraulic gradient should be calculated using flow lines. To simplify the calculation, the line of seepage flow in the dam was assumed to be along the yellow dotted line AB as shown in Fig. 4(a). Therefore, the average hydraulic gradient between PWP-1 and PWP-4 was approximate to the ratio of the difference between pore-water pressure 1 and 4 to the distance between these two transducers.

The rapid rise in pore-water pressures from the upstream side to the downstream side of the dam resulted in the development of a high seepage gradient that caused abrupt erosion and outwash of the dam materials to an exit point on the downstream face. This was evidenced by the rapid increase in turbidity of the effluent seepage to more than 400 NTU (about 55 h after the test beginning). From 60 to 95 h, the hydraulic gradient stayed almost the same, and the turbidity of the seepage water was as low as about 40 NTU. At about 95 h after the test beginning, the hydraulic gradient increased, triggering another peak

turbidity value of about 380 NTU. Therefore, the turbidity of seepage water could be an indicator of internal erosion through landslide dams, particularly in the early stages of the formation of the landslide dams.

3.2. Experiment 2

Fig. 13 shows the evolution of dam-crest settlement and the deformation behaviour of the dam model used in Experiment 2. The critical moments marked by T_A, T_B, T_C and T_D in the figure correspond to the four periods shown in Fig. 10. The dam material was partially saturated prior to the filling of the upstream reservoir. The build-up of significantly high pore-water pressures and the subsequent reduction of the effective stress of the soil in the periphery of the drainage channel initiated minor deformation of the dam body (critical moment T_A). The internal erosion process progressed into piping. The evidence is the gradual outwash of hyperconcentrated flows from a poorly developed hole at the toe of the downstream face. This was followed by a gradual settlement of the dam crest (critical moment T_B). The erosion processes led to the further deformation of the dam that resulted in the cracks near the dam crest (critical moment T_C). It is interesting to note that the outwash of the fluidized sediments from the evolving pipe coincided with the dam-body deformation recorded by the strain gauges. When the piping hole and cracks developed to a certain extent, the settlement of the dam crest suddenly increased, indicating the failure of the dam model (critical moment T_D).

The relationship between the vertical deformation of the dam body and dam-crest settlement is shown in Fig. 13. Before critical moment T_B, the height of the dam stayed at almost the same value and the vertical deformation of the dam body was approximately equal to zero at that time. After critical moment T_B, the crest settlement increased rapidly, and the vertical deformation increased at the same time. After critical moment T_D, both vertical deformation and crest settlement began to stabilize. Therefore, the variation in the vertical deformation of the dam body basically corresponded to that of the crest settlement.

Based on the curve fitting, the settlement curve can be fitted to time by a cubic polynomial equation, as shown in Fig. 13. For example, the relationship between S_d-Right and time can be expressed as $S = -0.0029\,t^3 + 0.0158\,t^2 - 3.7968\,t + 6.2043$, and the relationship between S_d-Central and time can be expressed as $S = -0.0164\,t^3 + 0.6976\,t^2 - 12.5840\,t + 8.5470$ (the units of settlement S and time t are millimetres and hours, respectively).

Fig. 14 shows the relationship between seepage-flow turbidity and settlement behaviour of the dam crest. At the beginning of the experiment, there was almost no obvious settlement on the dam crest, and the turbidity of the effluent seepage was lower than 55 NTU. Between critical moments T_A and T_B, the turbidity fluctuated slightly. After critical moment T_B, the turbidity value increased from 55 NTU to about 70 NTU, marking the early onset of seepage in the dam. At this moment, the dam-crest settlement increased rapidly. This was followed by a rapid increase in seepage-flow turbidity, indicating the progression of piping and internal erosion through the dam (critical moment T_C). The rate of enlargement of the piping hole under intense erosion can be directly related to the gradual settlement of the dam crest due to the removal of the underlying material. The pipe enlargement process reached its peak with a sharp increase in the dam-crest settlement, which corresponded to high turbidity values ranging from 350 to 400 NTU (critical moment T_D).

3.3. Experiment 3

Fig. 15 shows the time-series data for vertical deformation of the dam body (curves *VD*-1, *VD*-2 and *VD*-4) and dam-crest settlement (curves S_d-Central and S_d-Right) recorded in Experiment 3. Similar to those in Experiment 2, the settlement curves could be fitted to time by cubic polynomial equations, as shown in Fig. 15. The gradual rise in the reservoir level and the subsequent increase in pore-water pressures

(a)
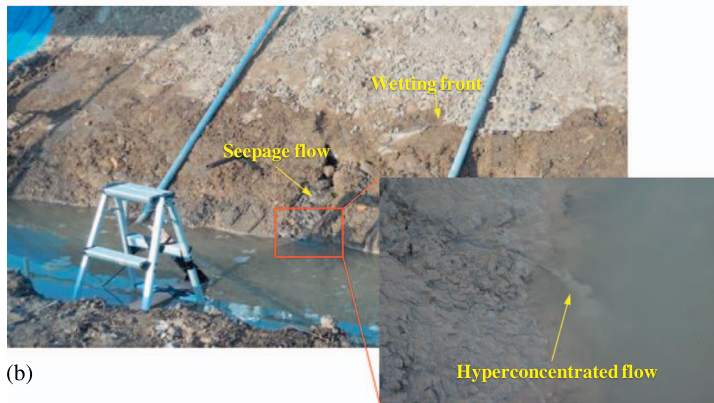
(b)

(c)

(d)

Fig. 10. Failure sequence of the landslide dam in Experiment 2: (a) seepage water at the downstream face at T_A; (b) hyperconcentrated flow from drainage channel at T_B; (c) emergence and evolution of cracks on the dam crest at T_C; (d) settlement of the dam crest and sudden collapse of the dam body at T_D.
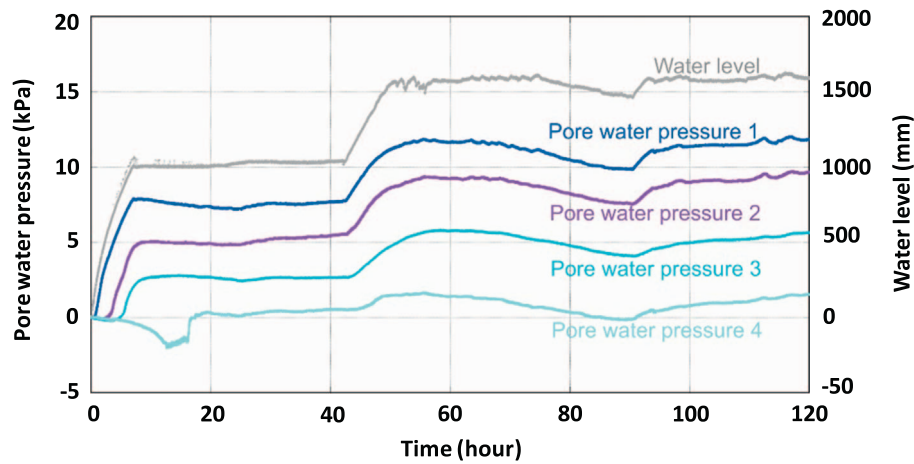
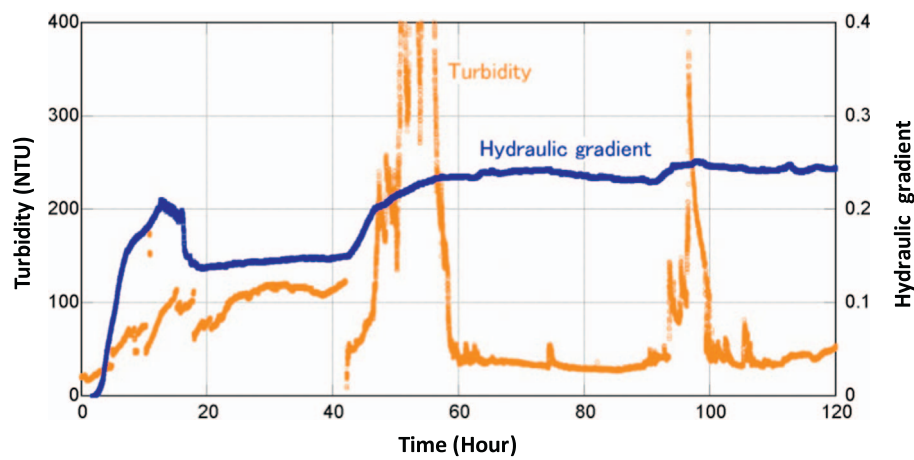**Fig. 11.** Evolution of the upstream water level and pore-water pressure in Experiment 1.

Fig. 12. Evolution of the hydraulic gradient and variation in turbidity of the seepage water in Experiment 1.
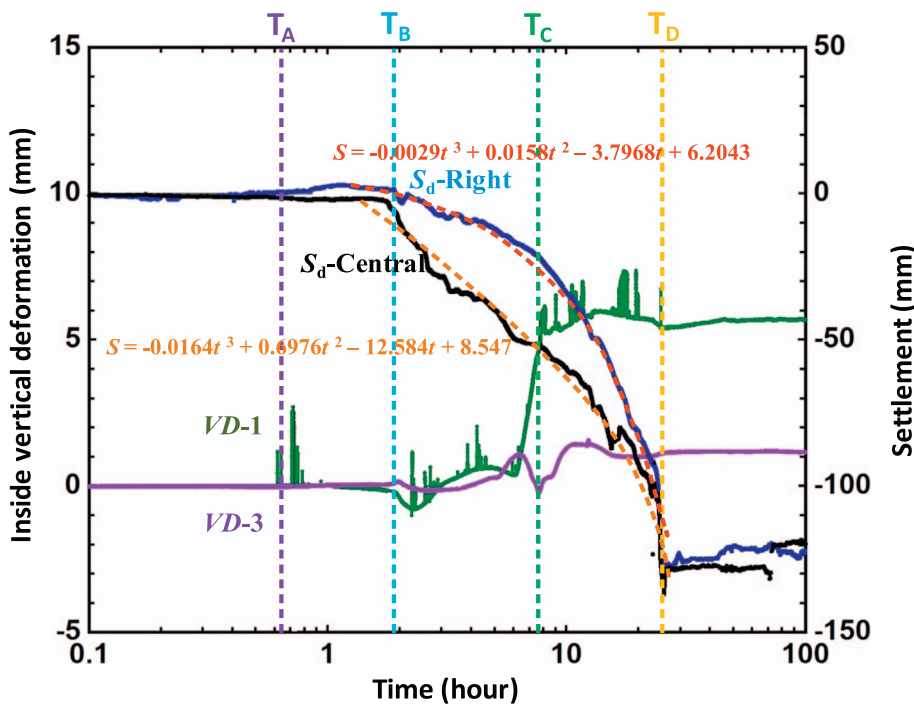

Fig. 13. Evolution of the dam-crest settlement S_d and the vertical deformation VD of the dam in Experiment 2.
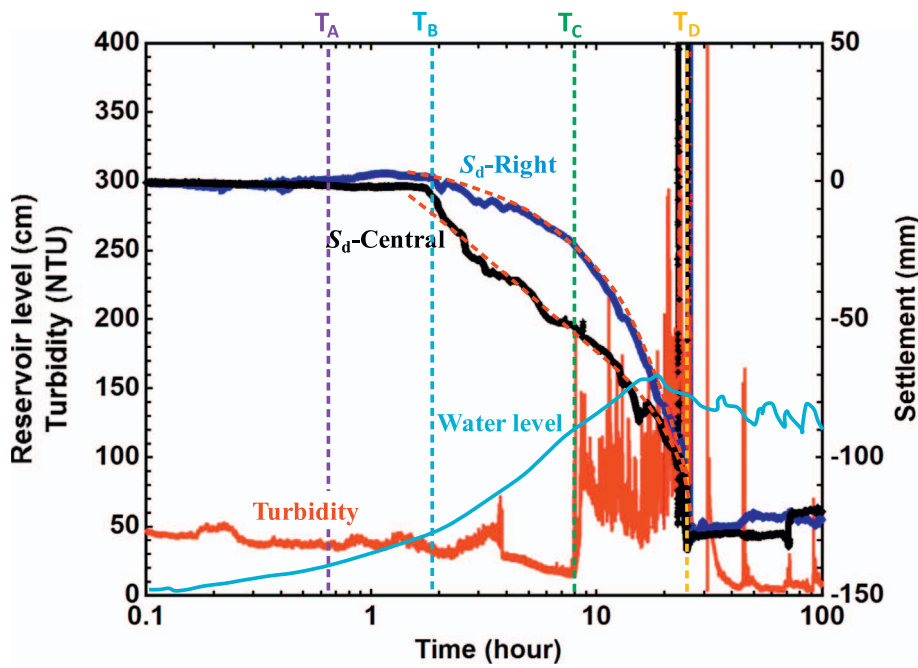
caused internal stress redistribution, which resulted in the formation of concave upward depressions (settlements) on the dam crest (critical moment T_A in Fig. 15). Early onset of internal deformation was detected via the strain of the pipe to which the four strain gauges were attached. It is estimated that the increase in seepage gradient around the artificial drainage channel triggered particle mobilization and entrainment, resulting in further redistribution of internal stresses as recorded by the strain gauges (critical moment T_B in Fig. 15). The vertical deformation inside the dam was measured through the strain gages on the upper surface of the PVC pipe. When the dam body vertically deformed due to the internal erosion, the PVC pipe bent in a vertical direction. However, the boundaries affected the deformation of the PVC pipe at both ends, which may have resulted in the deviation of the vertical deformation recorded by *VD*-1 and *VD*-4. Therefore, the vertical deformation behaviours in Figs. 13 and 15 are slightly different.

The onset of internal erosion was marked by the emergence of very turbid seepage water from the downstream toe and a sharp increase in the turbidity of the seepage water from 40 NTU to 270 NTU (critical moment T_C in Fig. 16). Consequently, the saturation of the downstream face under seepage resulted in the gradual undercutting of the

downstream toe, leading to slope instability and progressive failure. This phenomenon can be linked to very high turbidity values (T_D in Fig. 16) caused by the erosion and downstream transport of the mobilized materials. The turbidity reading reached its maximum value at around 22 h after the beginning of the experiment. At this moment, the settlement rate of the dam crest (the slope in the time-series curve of S_d around 22 h) increased. Hence, it could be concluded that seepage and internal erosion were the primary triggers for the failure of the landslide dam model.

3.4. Experiment 4

The self-potential (SP) method is a passive and non-intrusive geophysical technique that measures the potential difference between any two points on the ground produced by the small, naturally-occurring electrical currents beneath the Earth's surface, which possibly responses to subsurface fluid paths through the mechanism of streaming potential. Streaming potential is an electrokinetic process that describes the interaction between subsurface fluid path and electric flow within a porous rock mass or a saturated soil (Glover et al., 2012; Jouniaux and
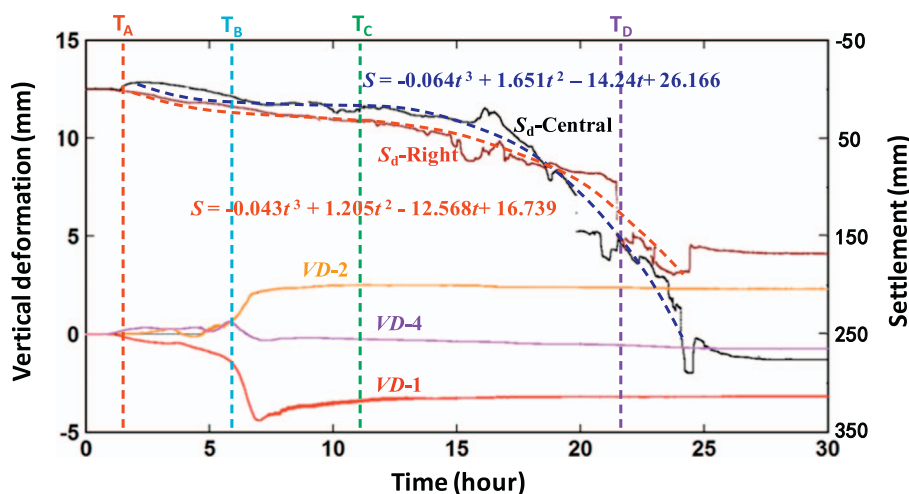
In the figure: $S = -0.064t^3 + 1.651t^2 - 14.24t + 26.166$ and $S = -0.043t^3 + 1.205t^2 - 12.568t + 16.739$
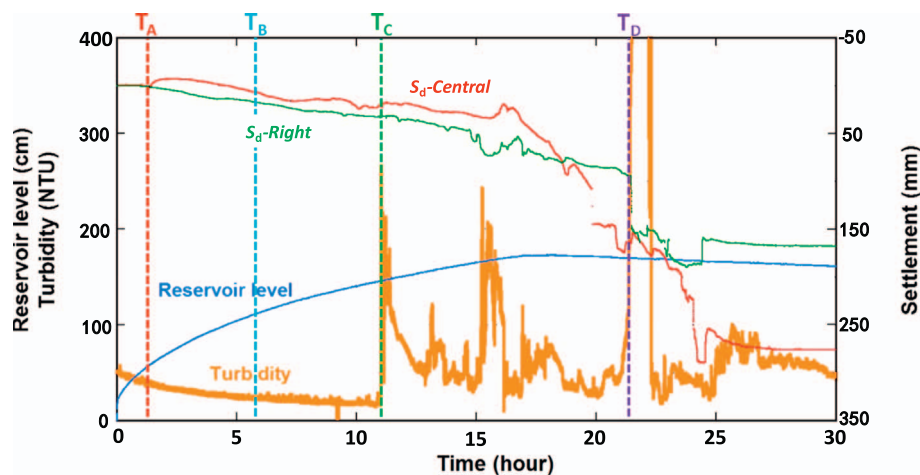
Fig. 16. Time-series data for the turbidity of seepage water and dam-crest settlement S_d in Experiment 3.
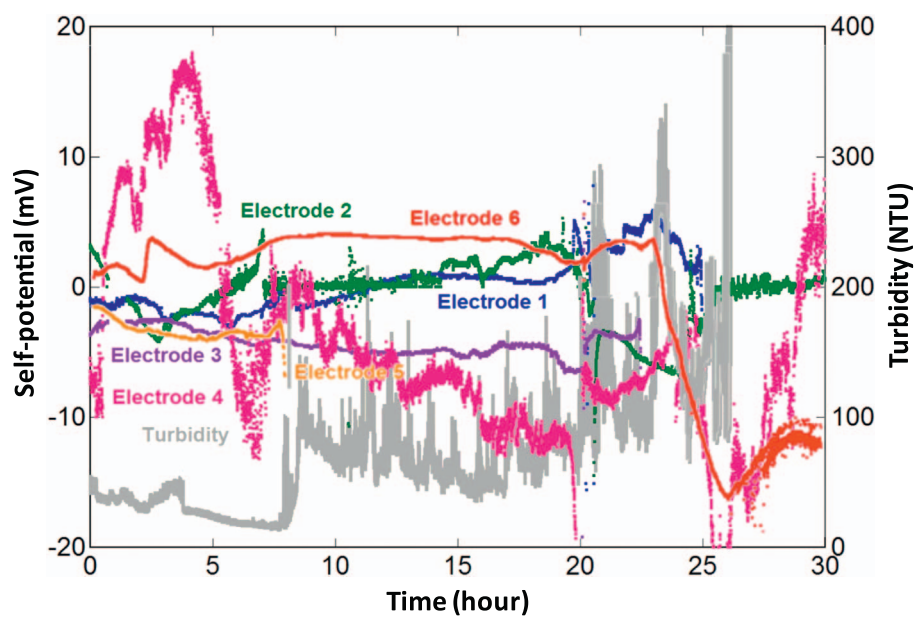

Fig. 17. Time-series data for the self-potentials at electrodes 1–6 and turbidity of seepage water in Experiment 4.
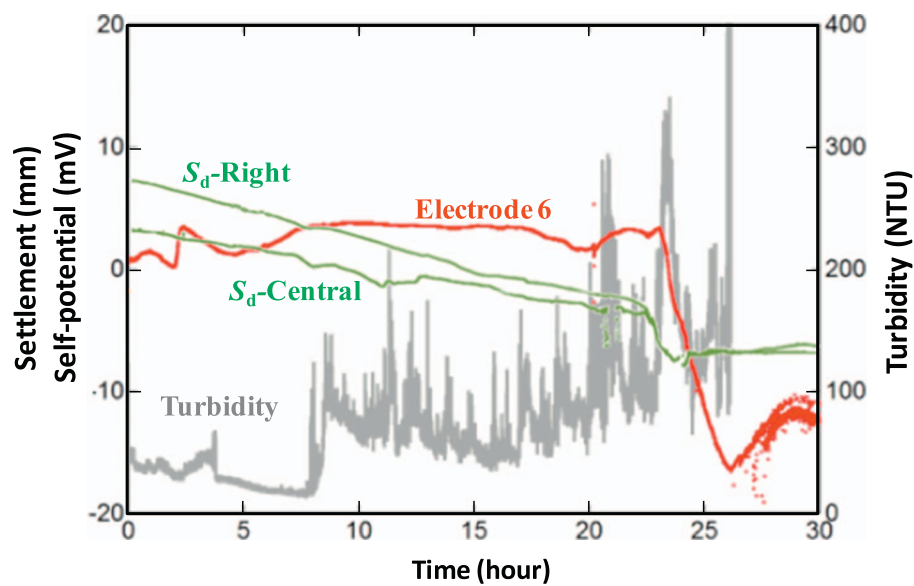

Fig. 18. Time-series data for the self-potential at Electrode 6, dam-crest settlement S_d and turbidity of seepage water in Experiment 4.

Ishido, 2012). This method is widely used in identifying seepage in dams and reservoirs (Al-Saigh et al., 1994; Panthulu et al., 2001; Bolève et al., 2009). Fig. 17 shows the variations in self-potential value and turbidity in Experiment 4. Self-potential ranged from − 20 mV to 18 mV during the test. After 7.5 h, the turbidity of the seepage flow started to increase. At this moment, the self-potential value gradually decreased (see curve for Electrode 4 in Fig. 17). When the self-potential value reached its minimum (around 26 h after the beginning of the test), the turbidity of the seepage flow reached a peak. Since Electrode 4 and Electrode 6 were positioned over the subsurface flow paths (the artificial drainage channel and the boundary), the self-potential responses measured by these two electrodes were more pronounced than the others.

Fig. 18 shows the relationship between self-potential of Electrode 6, seepage-water turbidity and dam-crest settlement in Experiment 4. Variation trends in the self-potential, turbidity and dam-crest settlement were approximately the same. At around 23 h after the beginning of the experiment, the dam-crest settlement increased sharply. At the same time, the self-potential dropped steeply from 2.4 mV to − 18 mV, and the turbidity increased. Therefore, the reasonable correspondence between the negative self-potential anomalies, the emergence of highly turbid hyperconcentrated flows on the downstream face and the dam-crest settlement gives credence to the notion that the self-potential changes could be regarded as one of the premonitory factors of the failure of the landslide dam model induced by seepage.

4. Conclusions

Large-scale (outdoor) experiments were conducted with the purpose of investigating the premonitory factors of landslide dam failure. The experimental scheme and the results indicated the significance of using precision sensors (pore-water pressure transducers, strain gauges, laser displacement sensors and turbidity sensors) in combination with non-invasive geophysical techniques (self-potential) in monitoring the performance of landslide dam models until final failure to predict landslide dam failure. The conclusions drawn from this study are described below.

Based on the changes in dam-crest settlement, seepage-water turbidity, vertical deformation inside the landslide dam and self-potential across the dam crest, and on the observations made during the tests, the failure sequence of the landslide dam model consisted of four sequential periods. In the first period, the monitoring parameters basically remained unchanged, seepage water emerged at the downstream face, and the turbidity of the seepage water was low. In the second period, the turbidity of the seepage water and the vertical deformation inside the dam body increased slightly. In the third period, cracks emerged and developed on the dam crest, and the dam-crest settlement increased. The turbidity of the seepage water varied greatly in this period. In the fourth period, the dam model suddenly collapsed when the self-potential dropped steeply and the dam-crest settlement reached a peak value.

The dam-crest settlement developed during the seepage in the landslide dam models. In the field investigations, the dam-crest settlement can be easily monitored using GPS or InSAR, and dam-crest settlement can therefore be used as an important factor in predicting landslide dam failure.

The variation in turbidity of the seepage flow correlated with the deformation behaviour of the landslide dam model, and a relationship between the turbidity trend and dam-crest settlement was found, meaning that the hyperconcentrated seepage flow could be regarded as a premonitory factor of the landslide dam failure. It must be noted that turbidity can only be used for landslide dams with rich fine particles at the early internal erosion stage. For a landslide dam subject to long-term piping and internal erosion, turbidity cannot be used because the transported particle size may become too large to form muddy water.

The self-potential (SP) method, a passive geophysical technique,

was applied to identify the seepage in the landslide dam models. The evolutionary self-potential trend was compared with the turbidity of the seepage flow, and a broadly negative relationship was found, indicating that self-potential could be effectively used to monitor subsurface flow that may cause internal erosion in landslide dams.

References

Al-Saigh, N.H., Mohammed, Z.S., Dahham, M.S., 1994. Detection of water leakage from dams by self-potential method. Eng. Geol. 37 (2), 115–121.
Amaya, P.J., Massey-Norton, J.T., Stark, T.D., 2009. Evaluation of seepage from an embankment dam retaining fly ash. J. Perform. Constr. Facil. 23 (6), 406–414.
Balmforth, N.J., Von Hardenberg, J., Provenzale, A., Zammett, R., 2008. Dam breaking by wave-induced erosional incision. J. Geophys. Res. Earth Surf. 113 (F1).
Balmforth, N.J., Von Hardenberg, J., Zammett, R.J., 2009. Dam-breaking seiches. J. Fluid Mech. 628, 1–21.
Bolève, A., Revil, A., Janod, F., Mattiuzzo, J.L., Fry, J.J., 2009. Preferential fluid flow pathways in embankment dams imaged by self-potential tomography. Near surface. Geophysics 7 (5–6), 447–462.
Bonelli, S., Benahmed, N., 2010. Piping flow erosion in water retaining structures: inferring erosion rates from hole erosion tests and quantifying the failure time. In: IECS 2010, 8th ICOLD European Club Symposium Dam Safety-Sustainability in a Changing Environment. ATCOLD Austrian National Committee on Large Dams 6p).
Bovis, M.J., Jakob, M., 2000. The July 29, 1998, debris flow and landslide dam at Capricorn Creek, mount meager volcanic complex, southern Coast Mountains, British Columbia. Can. J. Earth Sci. 37 (10), 1321–1334.
Brown, A.J., Gosden, J.D., 2008. Defra research into internal erosion. In: 15th British Dams Society Conference. Thomas Telford, Warwick.
Cao, Z., Yue, Z., Pender, G., 2011. Landslide dam failure and flood hydraulics. Part I: experimental investigation. Nat. Hazards 59 (2), 1003–1019.
Casagli, N., Ermini, L., 1999. Geomorphic analysis of landslide dams in the northern Apennine. Trans. Jpn. Geomorphol. 20, 219–249.
Costa, J.E., Schuster, R.L., 1988. The formation and failure of natural dams. Geol. Soc. Am. Bull. 100 (7), 1054–1068.
Costa, J.E., Schuster, R.L., 1991. Documented historical landslide dams from around the world. U.S. In: Geological Survey Open-File Report. 91-239. pp. 1–486.
Dai, F.C., Lee, C.F., Deng, J.H., Tham, L.G., 2005. The 1786 earthquake-triggered landslide dam and subsequent dam-break flood on the Dadu River, southwestern China. Geomorphology 65 (3), 205–221.
Daouadji, A., Darve, F., Gali, H.A., Hicher, P.Y., Laouafa, F., 2011. Diffuse failure in geomaterials: experiments, theory and modelling. Int. J. Numer. Anal. Met 35 (16), 1731–1773.
Dunning, S.A., Rosser, N.J., Petley, D.N., Massey, C.R., 2006. Formation and failure of the Tsatichhu landslide dam, Bhutan. Landslides 3 (2), 107–113.
Evans, S.G., 1986. The maximum discharge of outburst floods caused by the breaching of man-made and natural dams. Can. Geotech. J. 23 (3), 385–387.
Fell, R., MacGregor, P., Stapledon, D., Bell, G., 2005. Geotechnical Engineering of Dams. CRC Press (905 p).
Glover, P.W., Walker, E., Jackson, M.D., 2012. Streaming-potential coefficient of reservoir rock: a theoretical model. Geophysics 77 (2), D17–D43.
Hancox, G.T., McSaveney, M.J., Manville, V.R., Davies, T.R., 2005. The October 1999 Mt Adams rock avalanche and subsequent landslide dam-break flood and effects in Poerua River, Westland, New Zealand. N. Z. J. Geol. Geophys. 48 (4), 683–705.
Hermanns, R.L., Niedermann, S., Ivy-Ochs, S., Kubik, P.W., 2004. Rock avalanching into a landslide-dammed lake causing multiple dam failure in Las Conchas valley (NW Argentina)—evidence from surface exposure dating and stratigraphic analyses. Landslides 1 (2), 113–122.
Hewitt, K., 1982. Natural dams and outburst floods of the Karakoram Himalaya. IAHS 138, 259–269.
ICOLD, 2013. Internal Erosion of Existing Dams, Levees, and Dikes, and their Foundations, Bulletin 164 Preprint. International Commission on Large Dams, Paris, France.
Jouniaux, L., Ishido, T., 2012. Electrokinetics in earth sciences: a tutorial. Int. J. Geophys. 2012. http://dx.doi.org/10.1155/2012/286107.
King, J., Loveday, I., Schuster, R.L., 1989. The 1985 Bairaman landslide dam and resulting debris flow, Papua New Guinea. Q. J. Eng. Geol. Hydrogeol. 22 (4), 257–270.
Korup, O., Tweed, F., 2007. Ice, moraine, and landslide dams in mountainous terrain. Quat. Sci. Rev. 26 (25), 3406–3422.
Lade, P.V., 1992. Static instability, liquefaction of loose fine sandy slopes. J. Geotech. Engrg, ASCE 118 (1), 51–71.

Meyer, W., Schuster, R.L., Sabol, M.A., 1994. Potential for seepage erosion of landslide dam. J. Geotech. Eng. 120 (7), 1211–1229.

Nicot, F., Darve, F., Khoa, H.D.V., 2007. Bifurcation and second order-work in granular materials. Int. J. Numer. Anal. Methods Geomech. 31 (8), 1007–1032.

Nova, R., 1994. Controllability of the incremental response of soil specimens subjected to arbitrary loading programmes. J. Mech. Behav. Mater. 5 (2), 193–201.

O'Connor, J.E., Beebee, R.A., 2009. Floods from natural rock-material dams. In: Megaflooding on Earth and Mars, pp. 128–163.

Ojha, C.S.P., Singh, V.P., Adrian, D.D., 2008. Assessment of the role of slit as a safety valve in failure of levees. Int. J. Sediment Res. 23 (4), 361–375.

Panthulu, T.V., Krishnaiah, C., Shirke, J.M., 2001. Detection of seepage paths in earth dams using self-potential and electrical resistivity methods. Eng. Geol. 59 (3), 281–295.

Sherard, J.L., 1953. Influence of Soil Properties and Construction Methods on the Performance of Homogeneous Earth Dams. US Bureau of Reclamation Technical, Denver, pp. 199–201 Memo No.645.

Vilimek, V., Zapata, M.L., Klime, J., Patzelt, Z.E., Santillan, N., 2005. Influence of glacial retreat on natural hazards of the Palcacocha Lake area, Peru. Landslides 2 (2), 107–115.

Vorogushyn, S., Merz, B., Apel, H., 2009. Development of dike fragility curves for piping and micro-instability breach mechanisms. Nat. Hazards Earth Syst. Sci. 9 (4), 1383–1401.

Yan, J., Cao, Z.X., Liu, H.H., Chen, L., 2009. Experimental study of landslide dam-break flood over erodible bed in open channels. J. Hydrodyn. Ser. B 21 (1), 124–130.

Zhu, Y., Visser, P.J., Vrijling, J.K., 2006. Laboratory observations of embankment breaching. In: Proceeding of the 7th ICHE Congress. IAHR, ASCE, Drexel University. College of Engineering. DSpace Library. DU Haggerty Library, Philadelphia, USA.